American Mineralogist, Volume 104, pages 1381–1388, 2019

PO_4 adsorption on the calcite surface modulates calcite formation and crystal size

Yuki Sugiura[1,*,†], Kunio Ishikawa[2], Kazuo Onuma[3], and Yoji Makita[1]

[1]Health Environmental Control R.G., National Institute of Advanced Industrial Science and Technology (AIST), 2217-14, Hayashi-cho, Takamatsu, Kagawa 761-0395, Japan
[2]Department of Biomaterials, Faculty of Dental Science, Kyushu University, 3-1-1, Maidashi, Higashi, Fukuoka 812-8532, Japan
[3]Biomaterials R.G., National Institute of Advanced Industrial Science and Technology (AIST), 1-1-1, Higashi, Tsukuba, Ibaraki 305-8566, Japan

Abstract

Calcium carbonate ($CaCO_3$) and particularly its stable phase, calcite, is of great geological significance in the deep carbon cycle since $CaCO_3$ from biomineralized shells and corals form sedimentary rocks. Calcite also attracts attention in medical science and pharmacy as a primary or intermediate component in biomaterials because it possesses excellent biocompatibility along with suitable physicochemical properties. Calcite blocks have already been used during surgical procedures as a bone substitute for reconstructing bone defects formed by diseases and injury. When producing $CaCO_3$ biomaterials and bioceramics, in particular, in vivo control of the size and polymorphic nature of $CaCO_3$ is required. In this study, we investigated the effects of PO_4 on calcite formation during the phase conversion of calcium sulfate anhydrate ($CaSO_4$, CSA), which is sometimes used as a starting material for bone substitutes because of its suitable setting ability. CSA powder was immersed in 2 mol/L Na_2CO_3 solution containing a range of PO_4 concentrations (0–60 mmol/L) at 40 °C for 3 days. The treated samples were investigated by X-ray diffraction, Fourier-transform infrared spectroscopy, X-ray fluorescence spectroscopy, and thermal analysis. In addition, the fine structures of the treated samples were observed by field-emission scanning electron microscopy, and the specific surface area was measured. We found that PO_4, which is universally present in vivo, can modulate the calcite crystal size during calcite formation. A fluorescence study and calcite crystal growth experiments indicated that PO_4 adsorbs tightly onto the surface of calcite, inhibiting crystal growth. In the presence of high PO_4 concentrations, vaterite is formed along with calcite, and the appearance and stability of the $CaCO_3$ polymorphs can be controlled by adjusting the PO_4 concentration. These findings have implications for medical science and pharmacology, along with mineralogy and geochemistry.

Keywords: Calcite, morphology, phosphate, phase transformation, fabrication, calcium carbonate; Biomaterials—Mineralogy Meets Medicine

Introduction

Calcium carbonate ($CaCO_3$) is of great geochemical significance due to its role in Earth's carbon cycle (Zeebe et al. 2008; Dasgupta and Hirschmann 2010; Swart 2015). Marine organisms such as corals and mollusks absorb huge amounts of CO_2 from the ocean and atmosphere to form $CaCO_3$ skeletons and shells (Beaufort et al. 2011; Takahashi et al. 2014; Swart 2015; Li et al. 2018). The remains of these organisms accumulate as sediments on the bottom of the ocean, where they become sedimentary rocks. This process helps to maintain Earth's climate and ocean chemistry (Zeebe et al. 2008; Swart 2015; Li et al. 2018).

Calcite, the most stable phase of $CaCO_3$, is an attractive material in cancer therapy and as a bone substitute because of its excellent biocompatibility (Guo et al. 2012; Magnabosco et al. 2015; Ishikawa et al. 2016). The chemical composition of calcite includes only Ca and CO_3, which are ordinary components of the human body, and well-formed calcite crystals. Both of these properties are advantageous for drug carriers. In addition, calcite quickly dissolves under acidic conditions. Since the lactic acid in cancer cells causes the surrounding areas to become somewhat acidic (Gillies et al. 2004; Crayton and Tsourkas 2011; Longo et al. 2016), calcite could be used in cancer therapy to achieve selective drug release around cancer cells with minimum side effects.

In dentistry and orthopedics, calcite is also an attractive starting or intermediate material of carbonate apatite [CO_3Ap: $Ca_{10-x}(PO_4)_{6-b}(CO_3)_c(OH)_{2d}$], which is the primary inorganic component of bone as well as a new bone substitute. The in vivo properties of CO_3Ap are much better than those of conventional bone substitutes such as hydroxyapatite [HAp: $Ca_{10}(PO_4)_6(OH)_2$] (Ishikawa 2010; Fujisawa et al. 2018; Hara et al. 2018; Ishikawa et al. 2018; Wang et al. 2018). CO_3Ap cannot be fabricated via sintering because it decomposes at temperatures above 700 °C. Therefore, CO_3Ap, especially CO_3Ap blocks, is fabricated via dissolution/re-precipitation (Rey et al. 1989; Liu et al. 2015; Ishikawa et al. 2018) by immersing calcite in PO_4-containing solution (Sunouchi et al. 2012; Ishikawa et al. 2018).

However, for fabricating CO_3Ap blocks using the above method, it is mandatory to achieve a complete reaction. Since

* E-mail: yuki-sugiura@aist.go.jp
† Special collection papers can be found online at http://www.minsocam.org/MSA/AmMin/special-collections.html.

0003-004X/19/0010–1381$05.00/DOI: https://doi.org/10.2138/am-2019-7015

CO_3Ap formation is a surface-mediated reaction, calcite likely remains at some parts of the surface. Kasioptas et al. (2011) reported that for the hydrothermal treatment of millimeter-sized calcite single crystals at 200 °C for two weeks, calcite was converted to apatite only to the depth of several hundred micrometers from the calcite surface. To fabricate commercial bone substitutes, several sizes of CO_3Ap and calcite blocks, which are precursors to CO_3Ap, are required.

To fabricate bone substitute materials, the calcite, which is an intermediate material of CO_3Ap, has been synthesized from calcium sulfate via dissolution–precipitation phase conversion (Lowmunkong et al. 2007; Ishikawa et al. 2017). Calcium sulfate exhibits excellent molding properties such as self-setting ability, stable and partial sintering capability at high temperature, and high solubility (Partridge and White 1929; Sun et al. 2015). Furthermore, calcium sulfate is also used as a bone substitute (OsteoSet) because of its biocompatibility (Winn and Hollinger 2000; Pförringer et al. 2018). Therefore, calcium sulfate is a suitable precursor material for CO_3Ap bone substitute. During the phase conversion of calcium sulfate to calcite, developing synthesis method with a high yield is essential for novel CO_3Ap bone substitute.

Two authors of this manuscript (Y.S. and K.O.) have investigated how PO_4 affects $CaCO_3$ formation and dynamics based on crystal growth and mineralogy (Sugiura et al. 2013, 2014, 2016) on the basis of biomineralization. Even relatively low concentrations of PO_4 (PO_4/Ca < 1/1000) can inhibit $CaCO_3$ formation, especially the formation of metastable vaterite. However, the effects of PO_4 on calcite formation and, particularly, on calcite crystal size remain unclear. In this study, we investigated the effects of PO_4 on calcite formation during the phase conversion from calcium sulfate anhydrate [CSA: $CaSO_4$], which is sometimes used as a starting material of phase conversion for CO_3Ap bone substitute.

Experimental methods

Phase conversion from CSA to calcium carbonate in various PO_4-containing solutions

All reagents were purchased from Wako Pure Inc., Japan. Calcium sulfate hemihydrate powder (CSH: $CaSO_4 \cdot \frac{1}{2}H_2O$) powder was burned at 800 °C for 12 h to fabricate CSA powder.

Na_2CO_3 and $(NH_4)_2HPO_4$ were dissolved in distilled water to make stock solutions of Na_2CO_3 (2.5 mol/L) and $(NH_4)_2HPO_4$ (0.1 mol/L). Na_2CO_3 solution (16 mL, 2.5 mol/L) and 0–4 mL of $(NH_4)_2HPO_4$ solution (0.1 mol/L) were mixed with various volumes of H_2O (0–4 mL) to obtain a total volume of 40 mL. The solution concentration was adjusted to 1.0 mol/L Na_2CO_3 and 0–60 mmol/L $(NH_4)_2HPO_4$.

CSA powder (1.36 g) was immersed in 40 mL of 2.0 mol/L Na_2CO_3 and 0–60 mmol/L $(NH_4)_2HPO_4$ solution. The mixtures were then treated at 40 °C for 3 days. The treated CSA powders were washed several times with distilled water and 99.5% ethanol and then dried at room temperature.

Material characterization

The phase compositions of the treated samples were evaluated by X-ray diffraction (XRD; MiniFlex600, Rigaku Co., Japan) at an acceleration voltage of 40 kV and a current of 15 mA using a Cu target. The 2θ step and range were 0.01° and 3–70°, respectively, and the scan rate was 5 °/m.

Chemical bonding in the samples was characterized by Fourier-transform infrared spectroscopy (FTIR; Nicolet NEXUS670, Thermofisher Scientific Co., U.S.A.) using a triglycine sulfate detector (32 scans, resolution = 2 cm^{-1}) with a GeSe attenuated total reflectance prism.

The specific surface areas of the samples were measured by low-temperature nitrogen adsorption (NOVA1200e, Quantachrome Instruments Japan Co., Japan) using the Brunauer–Emmett–Teller (BET) method (Brunauer et al. 1938). The samples were evacuated overnight at room temperature, and nitrogen was introduced in 11 pressure steps (P/P_0 = 0.05–0.30) at a temperature of –196 °C.

The fine structures of the samples were observed by field-emission scanning electron microscopy (FE-SEM; JSM-6700F, JEOL Co., Japan) at an acceleration voltage of 5 kV. Before observation, the samples were sputter-coated with Os to prevent surface charge accumulation.

The particle size distribution of the samples was measured from SEM micrographs of each sample obtained using the ImageJ program (National Institute of Health–NIH, Maryland, U.S.A.). To estimate the dispersion correctly, we obtained micrographs from at least five different fields of view and more than 2000 particles for each sample.

The P(PO_4) contents of the samples were measured by X-ray fluorescence spectroscopy (XRF; SEA2210, SII nanotechnology Co., Japan) at an acceleration voltage of 15 kV under vacuum conditions. The P(PO_4)/Ca ratio was calibrated using commercial reagents (calcium carbonate, dicalcium hydrogen phosphate dihydrate, and HAp).

The thermal stability of the samples was determined by thermogravimetry and differential thermal analysis (TG-DTA; ThermoPlus, TG8110, Rigaku Co., Japan). The heating rate was 10 °C/min up to 200 °C using Al_2O_3 as a standard. The heated samples for XRD measurements were obtained similarly as those obtained by the TG-DTA method.

Evaluation of PO_4^{2-} adsorption on the calcite surface

Flavin mononucleotide [FMN: $C_{17}H_{21}N_4O_9P$], a phosphate-bearing vitamin B_2 derivative (Iwaki Seiyaku Co., Japan), was used as a fluorescent PO_4 material.

The in situ observation system consisted of a homemade observation cell and a solution flow system, as described in Sugiura et al. (2014). Briefly, the observation cell comprised a glass slide and polypropylene tubes, which were positioned on a Si plate. To examine the adsorption behavior of FMN on the calcite surface, single-crystal Si wafers along the (001) face were also dipped into a 10 mmol/L solution of $CaCl_2$ and Na_2CO_3 for 2 h to form calcite crystals on the Si surface. The calcite-coated plates were subsequently washed in doubly distilled water and then dried.

The observation cell was placed on a fluorescence optical microscope (Olympus BX-53, Olympus, Tokyo, Japan) equipped with a fluorescence optical filter set (Omega Optical Filter Set XF71, Omega Optical U.S.A.). The excitation wavelength λ_e and fluorescence wavelength λ_f of FMN are 474 and 540 nm, respectively.

The dissolution solution of vaterite spherulites used in the flow system contained 10 mmol/L $NaHCO_3$. The dissolution solution of calcite crystals contained 10 mmol/L $NaHCO_3$ and 10 μmol/L FMN. These solutions were supplied into the observation cell at 2 mL/min for 1 h using a rotary pump.

Calcite crystal growth in the presence of PO_4 solution

Calcite substrates (1 × 2 × 2 mm) obtained from the Saidousho mine in the town of Kaharu in the Fukuoka prefecture of Japan were cleaved from a large single crystal of Iceland spar grade crystal immediately before the experiment started. The calcite substrate was soaked in ultrapure (18.2 MΩ) water for surface etching. The two of etched calcite substrates were immersed in 10 mL of 1 mmol/L Na_2CO_3–$CaCl_2$ with 10 mol/L Na_2HPO_4 solution at room temperature for 3 and 12 h.

The surface of the calcite substrates was observed by atomic force microscopy (AFM: Nano Scope V, Bruker AXS Co., Japan) using a silicon cantilever (length = 125 μm, tip radius = 12 nm) at a scanning line frequency of 20 Hz in normal atmosphere conditions.

Results and discussion

The initial and final pH values of the treated solutions are shown in Figure 1. As $(NH_4)_2HPO_4$ concentration in solutions increases, both initial and final pH values of treated solutions slightly decreased.

Figure 2 shows the XRD patterns of CSA before and after immersion into solutions containing 2 mol/L Na_2CO_3 and various concentrations of $(NH_4)_2HPO_4$ at 40 °C for 3 days. In the pattern of the sample immersed in 2 mol/L Na_2CO_3 without $(NH_4)_2HPO_4$ (PO_4 free), all diffraction peaks can be attributed to calcite; the peak at ~29.4° corresponds to the (104) plane of calcite, while

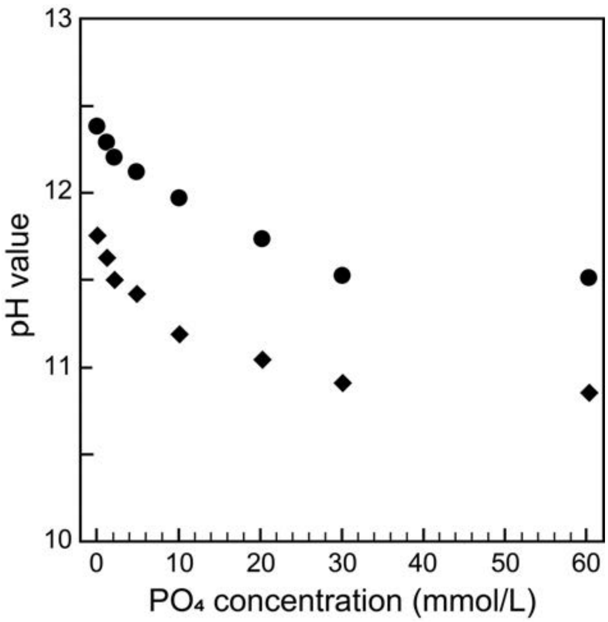

FIGURE 1. Initial and final pH values of treated solutions.

the peaks at 22.7°, 35.7°, and 39.1° correspond to the (012), (110), and (113) planes of calcite, respectively. This indicates that CSA was completely converted to monophasic calcite after immersion. Although monophasic calcite was obtained at PO_4 concentrations below 30 mmol/L, vaterite was observed along with calcite at PO_4 concentrations greater than 30 mmol/L, as indicated by the peaks at 27.4° and 32.4° corresponding to the (112) and (114) planes of vaterite, respectively. In summary, only calcite was formed at low PO_4 concentrations, whereas both calcite and vaterite were formed at high PO_4 concentrations.

The morphologies and fine structures of the samples were observed by SEM (Fig. 3). Before treatment, CSA exhibited rhombohedral crystals with sizes primarily in the range of several 10 μm (Fig. 3a). High-magnification observation revealed that surfaces of the rhombohedral crystals consisted of aggregated structures of granular crystals with sizes of approximately 1 μm (Fig. 3b). Therefore, these rhombohedral crystals were interpreted as mesocrystals with high porosity and unclear boundaries between granules. As shown in Figures 3c and 3d, the sample treated in PO_4-free solution exhibited rhombohedral crystals with sizes of 2–5 μm. Although some twinned crystals were observed, most of the particles showed the typical morphology of calcite with uniform crystal size. Figures 3e and 3f show SEM images of the sample treated with 2 mmol/L PO_4. While most of the crystals resembled those in the PO_4-free sample, approximately 10% of the crystals were fine particles with sizes of approximately 100 nm. Similar results were observed for the sample treated with 5 mmol/L PO_4, although the percentage of fine crystalline particles was higher (Figs. 3g and 3h). For the sample treated with 10 mmol/L PO_4, the SEM images (Figs. 3i and 3j) showed a small amount of rhombohedral crystals with a large number of fine particles with much smaller sizes than those observed in the samples treated with 2 and 5 mmol/L PO_4. No rhombohedral crystals were observed in the samples treated with PO_4 concentrations greater than 20 mmol/L; only particles with sizes on the order of 10 nm appeared in these samples (Figs. 3k and 3l).

The particle size distribution of the treated samples indicated the effect of PO_4 on calcium carbonate crystal growth. Figure 4 shows the particle size distribution of calcium carbonate crystals formed in various concentrations of PO_4. Except for the 0 and 60 mol/L PO_4 solutions, a bi-modal particle size distribution was observed. In addition, as the PO_4 concentration increased, the average size of the larger crystal decreased.

The bulk PO_4 effect on reducing calcium carbonate precipitation, which is shown by SEM was confirmed by specific surface area measurement of samples. Figure 5 shows the BET specific surface areas of the samples. As the concentration of PO_4 increased, the BET surface area increased linearly, consistent with the SEM observations.

Although the SEM observations revealed how PO_4 affected the morphologies and phases of $CaCO_3$, they did not provide information about how PO_4 affected the crystal structure of $CaCO_3$. We evaluated the crystal structure of calcite based on the strongest XRD peak, d_{104}. Peak shifting, which is indicative of alternation of the crystal lattice, was hardly observed because of its very unsystematic and slight variation (Fig. 6). This suggests that PO_4 was not significantly incorporated into the crystal

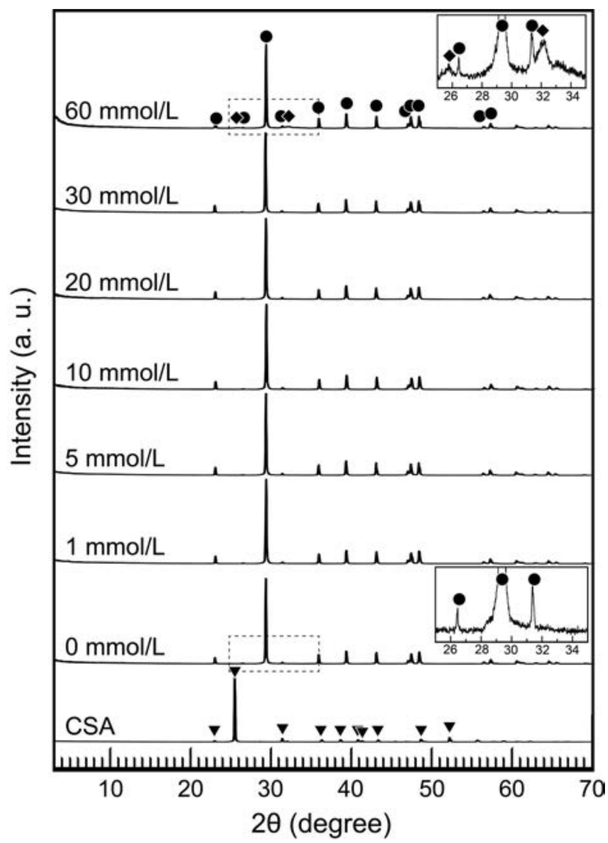

FIGURE 2. XRD patterns of CSA immersed into solutions containing 2 mol/L Na_2CO_3 and various concentrations of $(NH_4)_2HPO_4$ solutions at 40 °C for 3 days. The insets show magnified XRD patterns corresponding to the broken rectangular areas. Circles = calcite; diamonds = vaterite.

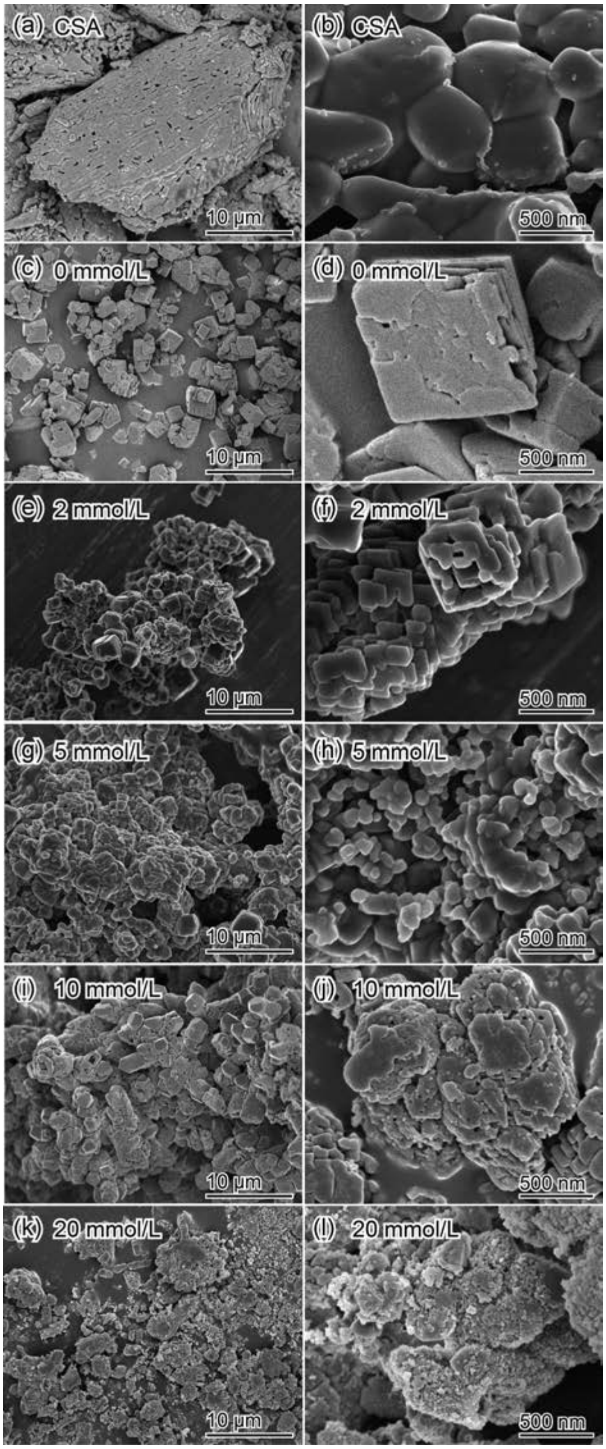

FIGURE 3. SEM micrographs of CSA (**a** and **b**) and CSA immersed into solutions containing 2 mol/L Na_2CO_3 with various concentration of PO_4 at 40 °C for 3 days. (**c** and **d**) 0 mmol/L, (**e** and **f**) 2 mmol/L, (**g** and **h**) 5 mmol/L, (**i** and **j**) 10 mmol/L, and (**k** and **l**) 20 mmol/L.

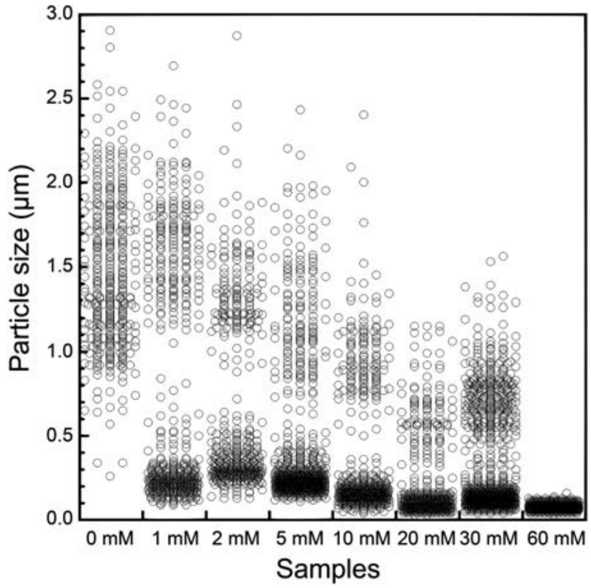

FIGURE 4. Particle size distribution of the samples.

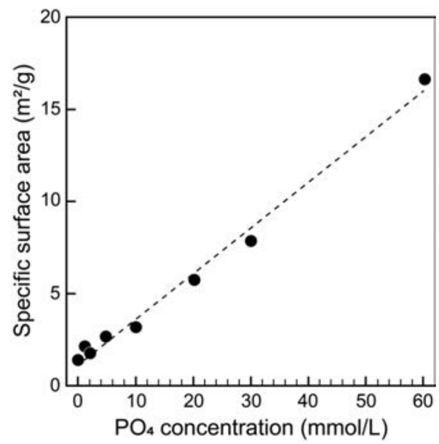

FIGURE 5. BET specific surface areas of the samples.

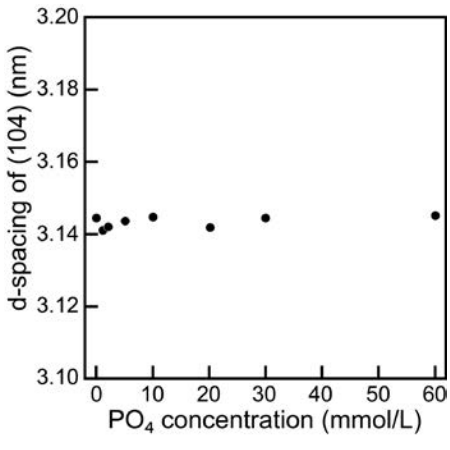

FIGURE 6. The *d*-spacings of the (104) plane of calcite for the samples treated with different concentrations of PO_4.

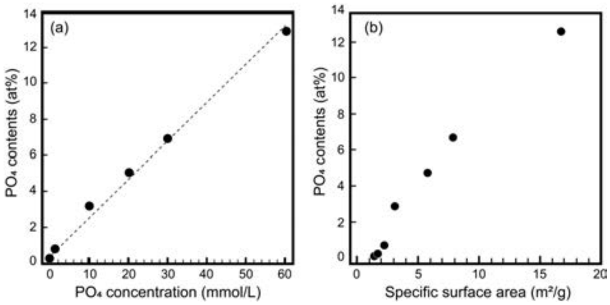

FIGURE 7. PO_4 contents of samples measured by XRF. (**a**) PO_4 concentration in treated solution vs. PO_4 content in samples. (**b**) Specific surface area of samples vs. PO_4 content in samples.

lattice of calcite. We also tried to measure the crystallite sizes of samples. However, we failed to observe any significant changes because the crystallinities of all samples, especially calcite, were too high to measure the crystallite size by the Scherrer and Rietveld methods.

The relationship between PO_4 concentration in the treatment solution and the PO_4 content in the samples was investigated. Figure 7 shows the PO_4 contents in the samples. The PO_4 contents of the samples increased linearly with increasing PO_4 content in the treatment solution (Fig. 7a). We also estimated the relation between surface area and PO_4 content (Fig. 7b). The trend between them was essentially the same as for PO_4 concentration in solution and PO_4 contents in samples. Indeed, it was shown that PO_4 could be present in calcite because of coprecipitation processes in nature (Otsuki and Wetzel 1972) and that a small amount of PO_4 could be incorporated into the calcite unit lattice by replacing CO_3 at weakly basic conditions (Ishikawa and Ichikuni 1981). However, in this study, at such strongly basic conditions, we considered that PO_4 could either be absorbed on the calcite surface or exist between the veins of calcite crystals rather than being substituted into the calcite unit lattice.

The chemical states of PO_4 in $CaCO_3$ were investigated by FTIR spectroscopy (Fig. 8). As PO_4 increases, the intensities of bands having high wavenumbers in the main adsorption peaks around 1350–1500 cm^{-1} increase (Fig. 8a). This indicated that the vaterite ratio in samples increased. These observed results coincided well with those of XRD results. The adsorption bands of PO_4 were too weak to be detected in the spectra of samples treated with PO_4 concentrations less than 10 mmol/L. In contrast, for the samples treated with PO_4 concentrations greater than 20 mmol/L, broad adsorption bands of PO_4 were observed (Fig. 8b). This adsorption band was split into bi-modal bands at 1028 and 1091 cm^{-1} in the spectrum of the sample treated with the highest PO_4 concentration (60 mmol/L), indicating the formation of a HAp-like structure. PO_4 was absorbed onto calcite and vaterite via different mechanisms.

The above results suggest that PO_4 adsorption onto the surface of calcite affects calcium carbonate formation. Therefore, we tried to evaluate the PO_4 adsorption ratio on the calcite surface. However, when calcite was immersed into PO_4 containing Na_2CO_3 solution, the adsorption ratio of PO_4 on the calcite surface by the washing process, which was essential for obtaining samples, was too small to accurately estimate it by atomic analyzing methods such as XRF and ICP. Therefore, we employed a visualization method using FMN as a PO_4-containing fluorescent material (Sugiura et al. 2014, 2015). Figure 9 shows calcite after treatment with an FMN-containing solution under normal light (9a) and fluorescent light (9b). The surface of calcite appeared bright under fluorescent light, indicating that PO_4 adsorbed onto the calcite surface.

We suggest that PO_4 adsorbs onto the calcite surface, thus affecting the calcite crystal growth. Hillocks formed on the cleaved calcite surface that grew in the PO_4 containing solution.

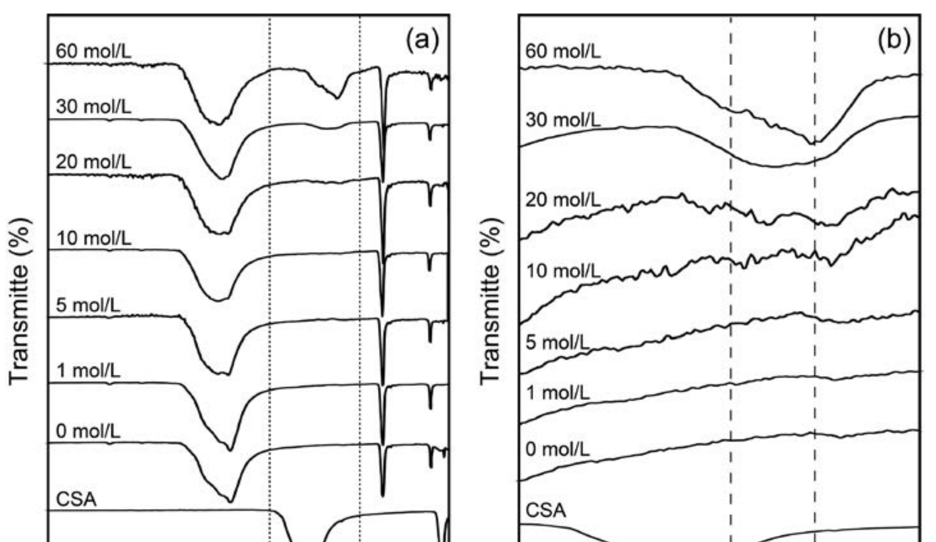

FIGURE 8. FTIR spectra of samples: (**a**) wide-range spectra and (**b**) PO_4 vibration region (the area indicated by the dotted lines in **a**).

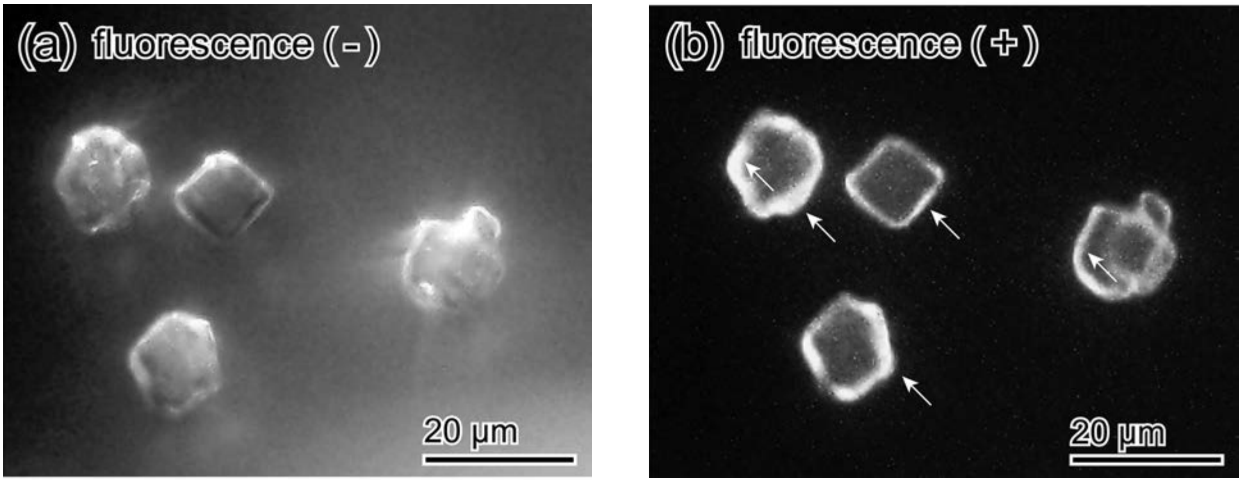

FIGURE 9. Fluorescent study of FMN (a PO_4-containing material) adsorption on calcite (**a**) normal light (without fluorescence) and (**b**) fluorescence light.

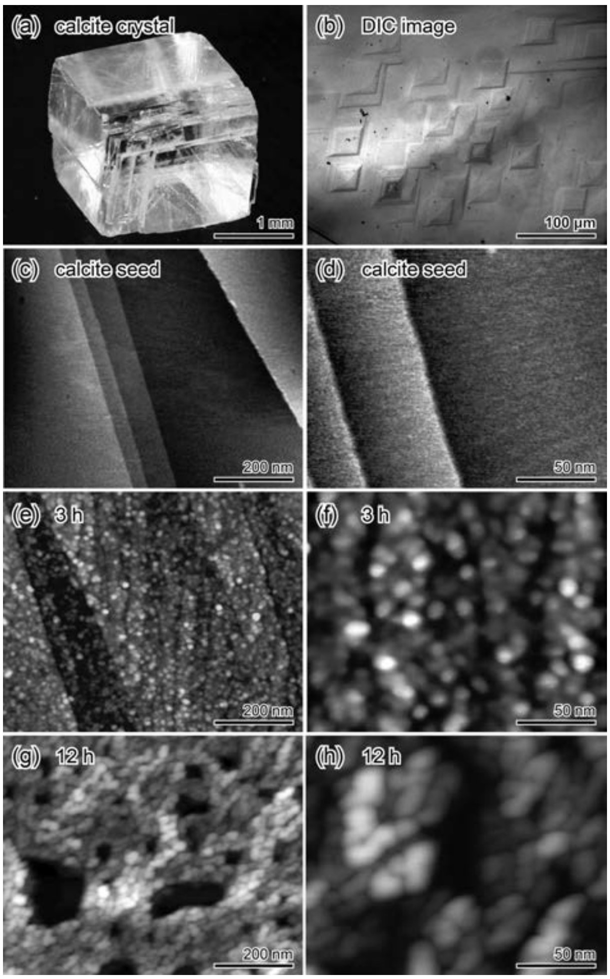

FIGURE 10. (**a**) Seeded calcite crystal. (**b**) Optical microscopic image of the cleaved calcite surface. AFM images of calcite crystal before cleavage (**c** and **d**) and after immersion in PO_4 containing a solution for 3 h (**e** and **f**) and 12 h (**g** and **h**).

When the cleaved calcite (Fig. 10a) was immersed in ultrapure water, typical etch pits formed on the cleaved surface (Fig. 10b). The AFM image shows that the etched calcite surface was essentially smooth (Figs. 10c and 10d). In contrast, when the cleaved calcite was immersed in the PO_4 containing solution, numerous particle structures ranging in size of several nanometers formed on the cleaved calcite surface instead of following a step-by-step growth (Figs. 10e and 10f). With increasing time, a porous structure comprising a complex accumulation of particle structures was formed (Figs. 10g and 10h).

Thermal analysis of samples revealed the sample decomposition process. Figure 11 shows the thermogravimetric analysis (TGA) curves of the samples. As seen in Figure 11a, all samples underwent a rapid decrease in weight above 700 °C, indicating calcite decomposition. The calcite decomposition temperature of the samples decreased slightly with increasing PO_4 concentration. In addition, we also observed the thermal behavior of the samples at lower temperatures. In Figure 11b, the TG curves of the samples up to 600 °C (i.e., below the calcite decomposition temperature) are presented. Without PO_4, very little weight loss was observed below 100 °C, suggesting that only a small amount of water adsorbed on the sample surface. As the PO_4 concentration increased, the weight loss of the samples below 100 °C also increased. Moreover, an additional weight loss at 200 °C was observed. Therefore, we suggest that PO_4 desorption occurred above 200 °C.

Previous studies indicated that the phase transformation from CSA to $CaCO_3$ occurs via dissolution/re-precipitation mediated by the aqueous environment (Nomura et al. 2014). In other words, CSA dissolves in the surrounding solution and releases Ca^{2+}, as described in Equation 1:

$$CaSO_4 \rightarrow Ca^{2+} + SO_4^{2-}. \quad (1)$$

This reaction occurred continuously until reaching the solubility of CSA; further, the reaction ceased after reaching the equilibrium. However, the treatment solutions in this study contained a large amount of CO_3^{2-} ions, and the solubilities of

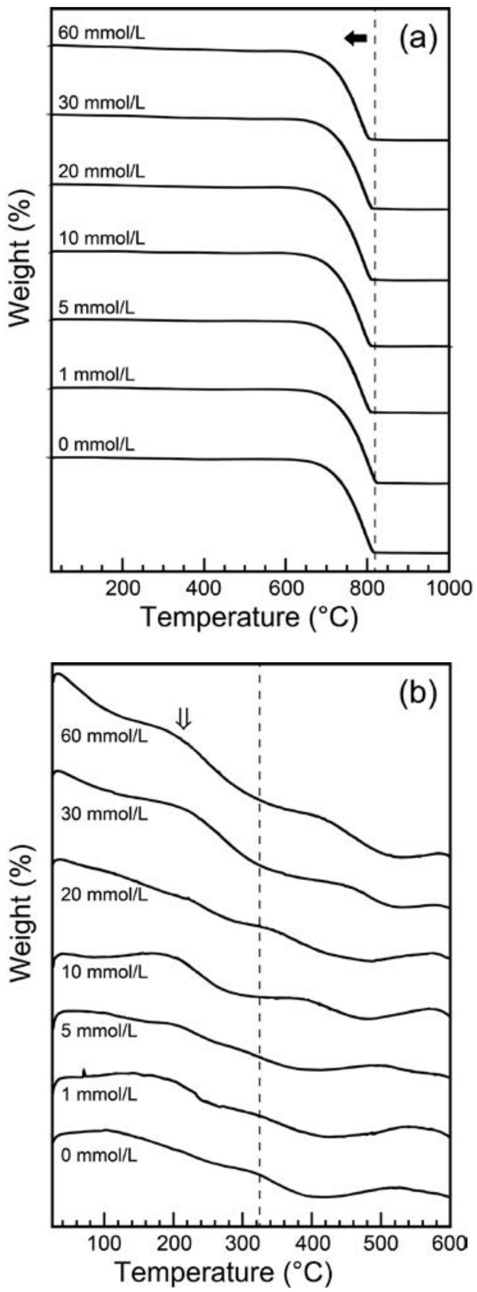

FIGURE 11. TG curve of the samples. (**a**) Room temperature to 1000 °C. (**b**) Room temperature to 600 °C. Left pointing arrow = The evidence of shifting toward to low temperature. Downward pointing arrow = The evidence of inflection point.

calcite and vaterite are lower than that of CSA (Dundon and Mack 1923; Partridge and White 1929; Plummer and Busenberg 1982). Therefore, the reaction described in Equation 2 also proceeds:

$$Ca^{2+} + CO_3^{2-} \rightarrow CaCO_3. \quad (2)$$

Equations 1 and 2 provide positive feedback to each other. Thus, these reactions proceed until CSA is used up, or until Ca^{2+} drops below the solubility of $CaCO_3$.

The results clearly indicate that PO_4 inhibits calcite growth and decreases its crystal size. Furthermore, treatment with high concentrations of PO_4 at high pH results in the formation of vaterite as opposed to calcite.

The fluorescent evaluation indicated that PO_4 could adsorb onto the surface of calcite. Thus, when calcite forms via ionic nucleation, PO_4 adsorbs onto the calcite surface, inhibiting calcite growth. This process also coincided with the results of a seeded calcite growth experiment. As a result, the concentration of Ca^{2+} and CO_3^{2-} ions was maintained in solutions containing PO_4 at supersaturated condition without precipitation. Thus, vaterite formed instead of calcite to thermodynamically stabilize the solution.

The results of this study contribute to the field of biomineralization by demonstrating that PO_4 can control $CaCO_3$ formation, polymorph, morphology, and crystal size. Our previous studies also indicated that PO_4 could control the kinetics of $CaCO_3$ formation in solution (Sugiura et al. 2013, 2014, 2016). $CaCO_3$ is thought to be the first mineral hard tissue formed after the birth of life in the Archean sea (Addadi et al. 2003). However, as life further evolved, vertebrate animals developed calcium phosphate-based hard tissues (Mann 2001; Addadi et al. 2003; Weiner and Dove 2003). These calcium phosphate hard tissues require vertebrate animals to store large amounts of PO_4 in their bodies because it is difficult to obtain PO_4 from the surrounding oceanic environment (Quekett 1849; Omelon et al. 2013). However, our finding may suggest that the reason why hard tissues of $CaCO_3$ were hardly formed in vertebrates is that their vivid metabolism causes large PO_4 fluctuations with high adenosine triphosphate (ATP) consummation.

IMPLICATIONS

The effects of PO_4 on $CaCO_3$ formation from CSA was investigated under high-pH conditions, at which calcite is likely to form. PO_4 regulates calcite formation and growth by adsorbing onto the surface of calcite. Therefore, under high PO_4 concentrations, calcite crystals become small and porous. In addition, vaterite is likely to form to counteract the thermodynamic instability of the solution. The results also indicate that PO_4, which is an essential component of CO_3Ap, can control the physico-chemical properties of $CaCO_3$, which is a precursor of carbonate apatite, a bone-replacement material (Ishikawa 2010; Ishikawa et al. 2018).

ACKNOWLEDGMENTS AND FUNDING

We thank Y. Uryu and T. Nakanishi for helping with FTIR measurement. This study is financially supported by priority issues of Health Research Institute, National Institute of Advanced Industrial Science and Technology (AIST) and, KAKENHI for Young Researcher (B), JP16K20505 and for Young Researcher, JP19H19081, respectively. This study is partially supported by the Research Center for Industrial Science & Technology, Kagawa Industry Support Foundation (RIST Kagawa).

REFERENCES CITED

Addadi, L., Raz, S., and Weiner, S. (2003) Taking advantage of disorder: amorphous calcium carbonate and its roles in biomineralization. Advanced Materials, 15, 959–970.

Beaufort, L., Probert, I., de Garidel-Thoron, T., Benedif, E.M., Ruiz-Pino, D., Metzl, N., Goyet, C., Buchet, N., Couple, P., Grelaud, M., Rost, B., Rickaby, R.E.M., and de Vargas, C. (2011) Sensitivity of coccolithophores to carbonate chemistry and ocean acidification. Nature, 479, 80–83.

Brunauer, S., Emmett, P.H., and Teller, E. (1938) Adsorption of gases in multi-

molecular layers. Journal of the American Chemical Society, 60, 309–319.
Crayton, S.H., and Tsourkas, A. (2011) pH-titratable superparamagnetic iron oxide for improved nanoparticle accumulation in acidic tumor microenvironments. ACS Nano, 5, 9592–9601.
Dasgupta, R., and Hirschmann, M.M. (2010) The deep carbon cycle and melting in Earth's interior. Earth and Planetary Science Letters, 298, 1–13.
Dundon, M.L., and Mack, E. Jr. (1923) The solubility and surface energy of calcium sulfate. Journal of American Chemical Society, 45, 2479–2485.
Fujisawa, K., Akita, K., Fukuda, N., Kamada, K., Kudou, T., Ohe, G., Mano, T., Tsuru, K., Ishikawa, K., and Miyamoto, Y. (2018) Compositional and histological comparison of carbonate apatite fabricated by dissolution–precipitation reaction and Bio-Oss®. Journal of Materials Science: Materials in Medicine, 29, 121–131.
Gillies, R.J., Raghunand, N., Garcia-Martin, M.L., and Gatenby, R.A. (2004) pH imaging. A review of pH measurement methods and applications in cancers. IEEE Engineering in Medicine and Biology Magazine, 23, 57–64.
Guo, Y.M., Zhang, J., Jiang, L.L., Shi, X.M., Yang, L., Fang, Q.L., Fang, H., Wang, K., and Jiang, K. (2012) Facile one-pot preparation of calcite mesoporous carrier for sustained and targeted drug release for cancer cells. Chemical Communications, 48, 10,636–10,638.
Hara, E.S., Okada, M., Nagaoka, N., Hattori, T., Kuboki, T., Nakano, T., and Matsumoto, T. (2018) Bioinspired mineralization using chondrocyte membrane nanofragments. ACS Biomaterials Science & Engineering, 4, 617–625.
Ishikawa, K. (2010) Bone substitute fabrication based on dissolution-precipitation reactions. Materials, 3, 1138–1155.
Ishikawa, M., and Ichikuni, M. (1981) Coprecipitation of phosphate with calcite. Geochemical Journal, 15, 283–288.
Ishikawa, K., Koga, N., Tsuru, K., and Takahashi, I. (2016) Fabrication of interconnected porous calcite by bridging calcite granules with dicalcium phosphate dihydrate and their histological evaluation. Journal of Biomedical Materials Research Part A, 104, 652–658.
Ishikawa, K., Kawachi, G., Tsuru, K., and Yoshimoto, A. (2017) Fabrication of calcite blocks from gypsum blocks by compositional transformation based on dissolution–precipitation reactions in sodium carbonate solution. Materials Science and Engineering C, 72, 389–393.
Ishikawa, K., Miyamoto, Y., Tsuchiya, A., Hayashi, K., Tsuru, K., and Ohe, G. (2018) Physical and histological comparison of hydroxyapatite, carbonate apatite, and β-tricalcium phosphate bone substitutes. Materials, 11, 1993–2004.
Kasioptas, A., Geisler, T., Perdikouri, C., Trepmann, C., Gussone, N., and Putnis, A. (2011) Polycrystalline apatite synthesized by hydrothermal replacement of calcium carbonates. Geochimica et Cosmochimica Acta, 75, 3486–3500.
Li, M., Song, H., Tian, L., Woods, A.D., Dai, X., and Song, H. (2018) Lower Triassic deep sea carbonate precipitates from South Tibet, China. Sedimentary Geology, 379, 60–71.
Liu, Q., Matinlinna, P., Chen, Z., Ning, C., Ni, G., Pan, H., and Darvell, B.W. (2015) Effect of thermal treatment on carbonated hydroxyapatite: Morphology, composition, crystal characteristics and solubility. Ceramics International, 41, 6149–6157.
Longo, D.L., Bartoli, A., Consolino, L., Bardini, P., Arena, F., Schwaiger, M., and Aime, S. (2016) In vivo imaging of tumor metabolism and acidosis by combining PET and MRI-CEST pH imaging. Cancer Research, 76, 6463–6470.
Lowmunkong, R., Sohmura, T., Takahashi, J., Suzuki, Y., Matsuya, S., and Ishikawa, K. (2007) Transformation of 3DP gypsum model to HA by treating in ammonium phosphate solution. Journal of Biomedical Materials Research Part B, 80(2), 386–393.
Magnabosco, G., Giosia, M.D., Polishchuk, I., Weber, E., Fermani, S., Bottoni, A., Zerbetto, F., Pelicci, P.G., Pokroy, B., Rapino, S., Falini, G., and Calvaresi, M. (2015) Calcite single crystals as hosts for atomic-scale entrapment and slow release of drugs. Advanced Healthcare Materials, 4, 1510–1516.
Mann, S. (2001) Biomineralization Principles and Concepts in Bioinorganic Materials Chemistry, Oxford University Press, U.K.
Nomura, S., Tsuru, K., Maruta, M., Matsuya, S., Takahashi, I., and Ishikawa, K. (2014) Fabrication of carbonate apatite blocks from set gypsum based on dissolution-precipitation reaction in phosphate-carbonate mixed solution. Dental Materials Journal, 33, 1–7.
Omelon, S., Ariganello, M., Bonucci, E., Grynpas, M., and Nanci, A. (2013) A review of phosphate mineral nucleation in biology and geobiology. Calcified Tissue International, 93, 382–396.
Otsuki, A., and Wetzel, R.G. (1972) Coprecipitation of phosphate with carbonates in a Marl Lake. Limnology and Oceanography, 17, 763–767.
Partridge, E.P., and White, A.H. (1929) The solubility of calcium sulfate from 0 to 200 °C. Journal of American Chemical Society, 51, 360–370.
Pförringer, D., Harrasser, N., Mühlhofer, H., Kiokekli, M, Stemberger, A., van Griensven, M, Lucke, M., Burgkart, R., and Obermeier, A. (2018) Osteoinduction and conduction through absorbable bone substitute materials based on calcium sulfate: in vivo biological behavior in a rabbit model. Journal of Material Science: Materials in Medicine, 29, 17–30.
Plummer, L.E., and Busenberg, E. (1982) The solubilities of calcite, aragonite and vaterite in CO_2-H_2O solutions between 0 and 90°C, and an evaluation of the aqueous model for the system $CaCO_3$-CO_2-H_2O. Geochimica et Cosmochimica Acta, 46, 1011–1040.
Quekett, J. (1849) On the intimate structure of bone, as composing the skeleton, in the four great classes of animals, viz., mammals, birds, reptiles, and fishes, with some remarks on the great value of the knowledge of such structure in determining the affinities of minute fragments of organic remains. Journal of Microscopy, 2, 46–58.
Rey, C., Collins, B., Goehl, T., Dickson, I.R., and Glimcher, M.J. (1989) The carbonate environment in bone mineral: A resolution-enhanced fourier transform infrared spectroscopy study. Calcified Tissue International, 45, 157–164.
Sugiura, Y., Onuma, K., Kimura, Y., Tsukamoto, K., and Yamazaki, A. (2013) Acceleration and inhibition effects of phosphate on phase transformation of amorphous calcium carbonate into vaterite. American Mineralogist, 98, 262–270.
Sugiura, Y., Onuma, K., Nagao, M., Momma, K., Kimura, Y., and Yamazaki, A. (2014) Dissolution behavior of vaterite spherulite in solutions containing phosphate ions. Journal of the Ceramic Society of Japan, 122, 679–687.
Sugiura, Y., Onuma, K., and Yamazaki, A. (2015) Solution chemical synthesis of hollow vaterite particles for advanced biomaterial applications. Chemistry Letters, 44, 20–22.
Sugiura, Y., Onuma, K., and Yamazaki, A. (2016) Growth dynamics of vaterite in relation to the physico-chemical properties of its precursor, amorphous calcium carbonate, in the Ca-CO_3-PO_4 system. American Mineralogist, 101, 289–296.
Sun, J., Wang, L., and Yu, G. (2015) Effects of Na, Ca, Mg, and Al chloride salts on dissolution and phase stability of calcium sulfate dihydrate in aqueous solutions at 278.15 K to 308.15 K. Journal of Chemical Engineering Data, 60, 2559–2566.
Sunouchi, K., Tsuru, K., Maruta, M., Kawachi, G., Matsuya, S., Terada, Y., and Ishikawa, K. (2012) Fabrication of solid and hollow carbonate apatite microspheres as bone substitutes using calcite microspheres as a precursor. Dental Materials Journal, 31, 549–557.
Swart, P.K. (2015) The geochemistry of carbonate diagenesis: The past, present and future. Sedimentology, 62, 1233–1304.
Takahashi, T., Sutherland, S.C., Chipman, D.W., Goddard, J.G., Ho, C., Newberger, T., Sweeney, C., and Munro, D.R. (2014) Climatological distributions of pH, pCO_2, total CO_2, alkalinity, and $CaCO_3$ saturation in the global surface ocean, and temporal changes at selected locations. Marine Chemistry, 164, 95–125.
Wang, M., Qian, R., Bao, M., Gu, C., and Zhu, P. (2018) Raman, FT-IR and XRD study of bovine bone mineral and carbonated apatites with different carbonate levels. Materials Letters, 210, 203–206.
Weiner, S., and Dove, P.M. (2003) An overview of biomineralization processes and the problem of the vital effect. In P.M. Dove, J.J. DeYoreo, and S. Weiner, Eds., Biomineralization, 54, 1–30. Reviews in Mineralogy and Geochemistry, Mineralogical Society of America, Chantilly, Virginia.
Winn, S.R., and Hollinger, J.O. (2000) An osteogenic cell culture system to evaluate the cytocompatibility of Osteoset®, a calcium sulfate bone void filler. Biomaterials, 21, 2413–2425.
Zeebe, R.E., Zachos, J.C., Caldeira, K., and Tyrrell, T. (2008) Carbon emissions and acidification. Science, 321, 51–52.

Manuscript received February 20, 2019
Manuscript accepted June 17, 2019
Manuscript handled by Robert Heimann